Mechanism and Machine Theory 79 (2014) 184–197

Contents lists available at ScienceDirect

Mechanism and Machine Theory

journal homepage: www.elsevier.com/locate/mechmt

Design of a two-stage cycloidal gear reducer with tooth modifications

Wan-Sung Lin [a], Yi-Pei Shih [b], Jyh-Jone Lee [a,*]

[a] Department of Mechanical Engineering, National Taiwan University, Taipei 106, Taiwan
[b] Department of Mechanical Engineering, National Taiwan University of Science and Technology, Taipei 106, Taiwan

ARTICLE INFO

Article history:
Received 2 September 2013
Received in revised form 11 April 2014
Accepted 16 April 2014
Available online 15 May 2014

Keywords:
Structural analysis
Two-stage cycloidal gear reducer
Tooth modification
Tooth contact analysis
Kinematic error

ABSTRACT

The cycloidal gear reducer is a compact, high-ratio, and low-backlash speed reduction device. It has been commonly used for transmitting motion and torque in machinery. This paper presents the design of a new two-stage cycloidal speed reducer with tooth modifications. The topological structure of cycloidal drives is discussed and analyzed with the aid of graphs. New cycloidal gear reducers are enumerated through the topological analysis and a new two-stage cycloidal gear reducer with simpler structure is then proposed. The design of the proposed cycloidal gear reducer is also performed, including profile generation and modifications. Subsequently, kinematic errors are analyzed by using the tooth contact analysis, and the results caused by different combinations of the gear profile modifications are presented quantitatively. Finally, based on the analysis, a mock-up of the cycloidal gear drive is constructed to validate the feasibility of the new mechanism.

1. Introduction

Cycloidal gear reducers (or cycloidal drives) are high-efficiency and high speed reduction ratio motion and torque transmission devices. They are commonly used in equipment where precise output and large drive payloads are needed. Recently, with the increasing demand of high efficiency and high speed reduction and torque ratio transmission devices in industry, applications of cycloidal gear reducers have become popular in the automation field as robotics, machine tools, and automatic machinery. Nonetheless, compared to involute gear drives, manufacture of cycloidal gear reducers requires a more dedicated process because of the non-standard characteristics of the devices. Further, tools for manufacturing cycloidal gears are not as specialized as for manufacturing involute gears. These features make accuracy control and cost reduction of manufacturing cycloidal drives a great challenging task. The research and development of the cycloidal gear reducers have been investigated by many researchers, including profile generation [1–6], conditions for non-undercutting manufacturing [7–9], manufacturing errors and their influence on output speed [10,11], force analysis and efficiency [12,13], and development of new mechanisms [14–17]. The early literature that studied cycloidal drives can be dated back to Botsiber and Kingston [1] and Pollitt [2] where the cycloidal speed reducer was initially introduced. Then, papers on cycloidal drives deal with the geometry and profile generation of the cycloidal disc. Other research considers profiles generated from different types of tooth [5]. Blanche and Yang [3] used a vector method to generate the cycloidal profile while Yan and Lai [4] approached the problem by means of the theory of conjugate surfaces. Hsieh [6] studied the epitrochoidal and hypotrochoidal profiles by the theory of gearing thoroughly. Fong and Tsay [7] and Hsieh and Hwang [8] derived the conditions for non-undercutting and obtained the constraint of parameters for non-undercutting. Sensinger [9] presented a unified approach to cycloidal drive profile, stress and efficiency with closed-form equations. Blance and Yang [10] investigated machining tolerances of cycloidal drives and their influence on output speed by means of instant centers. Huang [11] also studied the profile modification and

* Corresponding author. Tel.: +886 2 33662718.
E-mail address: jjlee@ntu.edu.tw (J.-J. Lee).

http://dx.doi.org/10.1016/j.mechmachtheory.2014.04.009
0094-114X/

Nomenclature

ω_i	angular velocity of link i
z_i	number of teeth of link i
m	speed reduction ratio
r_p	roller position
r_{rp}	radius of the roller
$\mathbf{r}_1$	position of P with respective to coordinate system 1
$\mathbf{r}_2$	position of P with respective to coordinate system 2
$\mathbf{M}_{ij}$	transformation matrix from system j to system i
a	eccentricity of crank
α	surface parameter of the point P on the roller
Δr_p	value of modification of roller position
Δr_{rp}	value of modification of roller radius
$\mathbf{n}_{c1}$	contact normal of the 1st-stage cycloidal disc
$\mathbf{n}_{r1}$	contact normal of the 1st-stage roller
$\mathbf{n}_{c2}$	contact normal of the 2nd-stage cycloidal disc
$\mathbf{n}_{r2}$	contact normal of the 2nd-stage roller

tooth contact analysis of the cycloidal drive. On the other hand, the development of new cycloidal drives can also be found in patent literature [14,15]. Li et al. [16] proposed a new drive for high load capacity. Blagojevic et al. [17] introduced a new two-stage cycloidal speed reducer of which speed reduction ratio was increased compared with the one-stage cycloidal drive. In view of the demand for the development of a new design, it can be seen that the development of a device with a higher speed reduction ratio, more compact size and high accuracy is continuing and indeed in need. Thus, the aim of this work is to address the development and design of a new two-stage cycloidal gear reducer. The cycloidal gear reducer from the topological view point is first investigated such that the structural characteristics can be further realized. Subsequently, new configurations of the two-stage structure are enumerated from the topological analysis and a new mechanism with simple structure is proposed. Then, the design of the proposed two-stage cycloidal gear drive with tooth modifications is performed by the theory of gearing [18]. The profile tolerances that compensate the errors of assembly and manufacturing will also be studied. The kinematic errors caused by the tooth modifications are simulated via tooth contact analysis. Finally, a mock-up of the device is constructed to validate the feasibility of the new mechanism.

2. Structural analysis of the cycloidal gear reducer

As shown in Fig. 1, the conventional one-stage gear reducer mainly consists of the case (1) (as fixed frame), crank (2), cycloidal disc (3) and output disc (4). When operating, the input crank deflects the cycloidal disc such that the cycloidal disc orbits and wobbles about the center of the crank shaft because of the crank's eccentricity and meshing between the disc and rollers on the case. Since the motion of the cycloidal disc is epicyclic and wobbling, it is necessary to convert such motion to pure

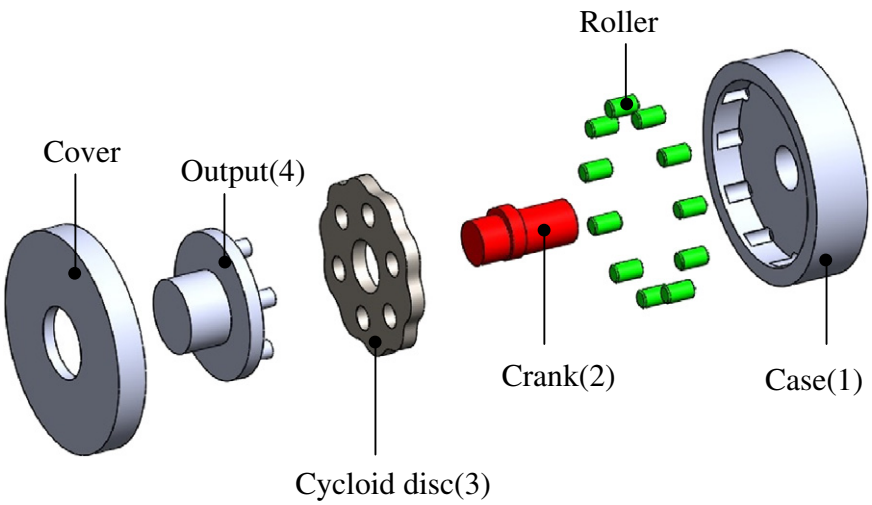

Fig. 1. Main structure of the conventional one-stage cycloidal gear reducer.

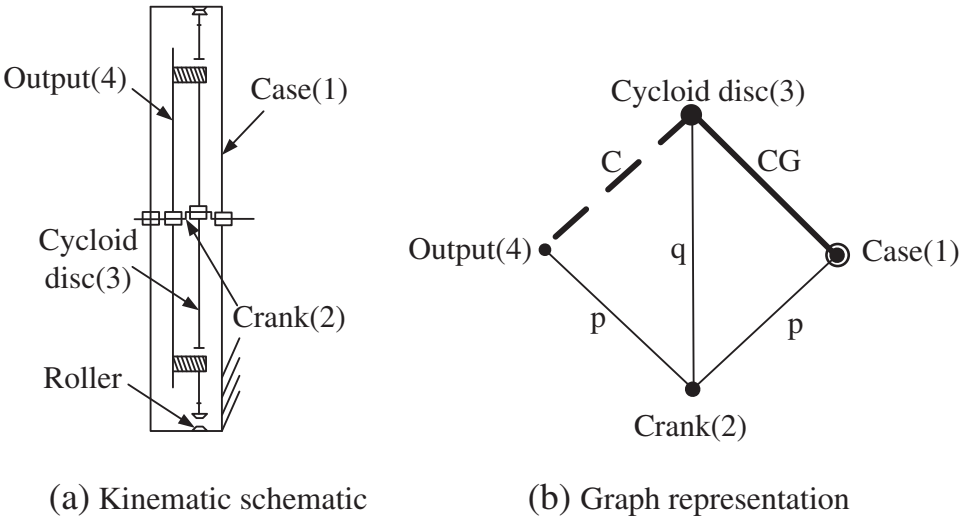

Fig. 2. One-stage cycloidal gear reducer.

rotation motion of the output disc about a fixed axis. This can be accomplished by intruding the pin (fixed on the output disc) into the hole on the cycloidal disc such that the kinematic paring between the pin and the circumference of the hole is molded as a cam pair (see Fig. 2a). Therefore, when represented in a graph, the topology of the mechanism can be depicted as shown in Fig. 2(b).

In the graph representation, the vertex represents the link, the thin edge represents the turning pair, the heavy edge represents the cycloidal gear pair (CG), the heavy dashed edge represents the cam pair (C), and p, and q represents different levels of the axis of rotation. The graph representation of the gear reducer can quickly help the designer realize the essential topological information about which link is connected to which other links by what types of joints and can be used for enumerating new structures if necessary [19–21]. When observing the graph representation of the one-stage cycloidal gear reducer, it can be seen that a different topological structure can be obtained by applying the structural synthesis methodology in [19,20], if the joint connecting links 3 and 4 is relabeled to a cycloidal gear pair as shown in Fig. 3(a). This topological structure when depicted in a kinematic schematic as shown in Fig. 3(b), becomes a two-stage cycloidal gear reducer. In practice, since the cycloidal disc is mounted on a shaft with eccentricity, an equal-mass counter balancer must be installed on the shaft 180° opposite to the cycloidal disc to retain dynamic balance when operating [22]. However, a more effective method for resolving the balancing issue in the gear drive can be conceived from the topological representation of Fig. 3(a) [21]. In view of Fig. 3(a), let the cycloidal disc first be divided into two discs 3 and 3′ of equal mass and then placed at an identical radius (eccentricity), 180° apart rotationally on the shaft. Then a pin element fixed to link 3′ is

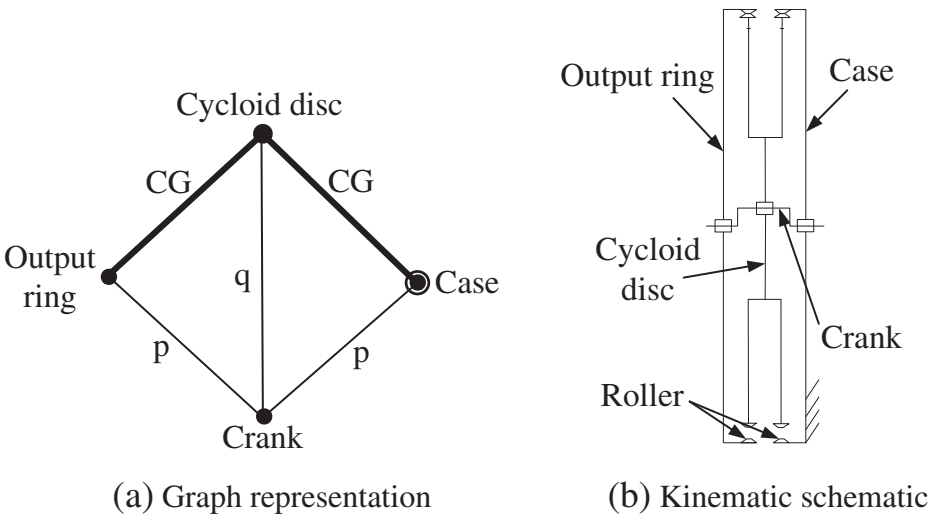

Fig. 3. A two-stage cycloidal gear drive.

used to transmit the epicyclic motion of link 3 to 3′ via cam pairing between pin and link 3 such that the rotational speeds of two cycloidal discs are identical. Finally, an output ring (4) is made to mesh with cycloidal disc 3′ via cycloidal gear pair and serves as the output link. Consequently, the kinematic schematic can be depicted as shown in Fig. 4(a) and the corresponding graph representation is shown in Fig. 4(b).

Furthermore, if the cam pair between links 3 and 3′ is replaced by a link and two turning pairs at both ends according to the rules of generalization of a generalized joint in [20], a new kinematic structure can also be obtained. The kinematic schematic and corresponding graph representation are respectively shown in Fig. 5(a) and (b). It should be noted that if such a mechanism is to be designed, the offset distance between the two turning joint axes on the cycloidal discs should be twice as large as the eccentricity of the cycloidal disc on the crank. From the graph representation Fig. 4(b), it can also be seen that crank 2 serves as the carrier for the two cycloidal gear train units 3–1–2 (first stage) and 3′–4–2 (second stage). The two train units comprise a non-fractionated mechanism [19], which is different from the structure of two gear trains in serial connection. Comparing the structure of Fig. 4(a) with that of Fig. 3(b) (or in [22]), the two structures have the same number of links except that the former does not need additional counter-balance weight. Therefore, a lighter and more compact structure than that of Fig. 3(b) can be obtained. In addition, after comparing Fig. 4(a) with the structure in [17], the motion of the first stage cycloidal disc in Fig. 4 is transferred to the second stage cycloidal disc via cam pairing without going through an intermediate plate. This leads to a reduction of number of links and cam pairs. Hence, a lighter, more compact configuration, and less wearing in the whole structure can be obtained. In what follows, to validate the feasibility of the mechanism, the design and the error analysis of this mechanism will be conducted.

The angular velocity analysis of the mechanism shown in Fig. 4(a) can be easily conducted using the angular velocity analysis method of the epicyclic gear trains. Let ω_1, ω_2, ω_3, ω_3', and ω_4 respectively represent the angular velocities of the case (1), crank (2), first stage cycloidal disc (3), second stage cycloidal disc (3′) and output ring (4). Since crank 2 serves as the carrier for the first stage cycloidal train unit 3–2–1 and second stage cycloidal train unit 3′–2–4, the angular velocity relation can be written for each train unit as:

$$\frac{\omega_3-\omega_2}{\omega_1-\omega_2}=\frac{z_1}{z_3} \tag{1a}$$

$$\frac{\omega_3'-\omega_2}{\omega_4-\omega_2}=\frac{z_4}{z_3'} \tag{1b}$$

where z_1 and z_4 are respectively the number of rollers on the case and output ring; z_3 and z_3' are respectively the number of teeth (lobes) on the 1st-stage and 2nd-stage cycloidal discs. Meanwhile, the case is fixed as the frame, $\omega_1 = 0$, and the angular velocity of the 1st-stage cycloidal disc is equivalent to that of the 2nd-stage cycloidal disc, $\omega_3 = \omega_3'$. After substituting these conditions into Eq. (1a) and (1b) and rearranging, the speed reduction ratio m can be derived as:

$$m=\frac{\omega_{in}}{\omega_{out}}=\frac{\omega_2}{\omega_4}=\frac{1}{1-\frac{z_1 z_3'}{z_3 z_4}}. \tag{2}$$

Theoretically, if the ratio $(z_1 z_3'/z_3 z_4)$ in the denominator of Eq. (2) approaches one, the speed reduction ratio m can become very large. In case a one-tooth difference between the cycloidal disc and the mating ring is applied, i.e., $z_1 = z_3 + 1$ and $z_4 = z_3' + 1$, the speed reduction ratio m can be further simplified as:

$$m=\frac{z_3 z_3'+z_3}{z_3-z_3'}. \tag{3}$$

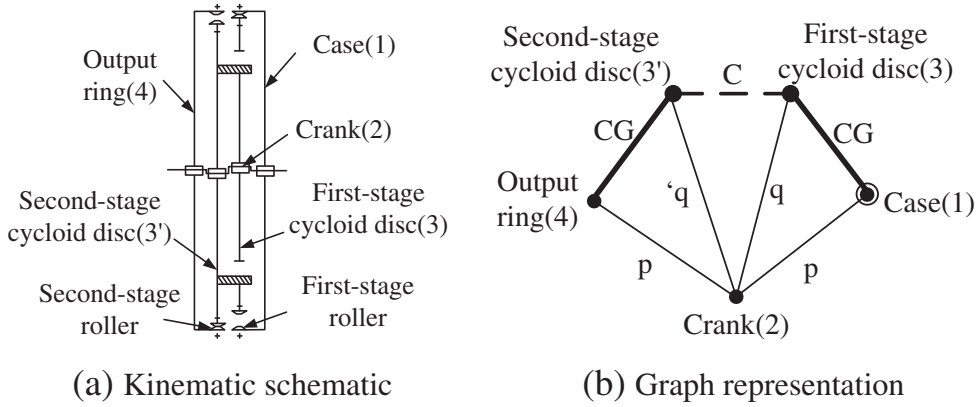

Fig. 4. A new two-stage cycloidal gear reducer.

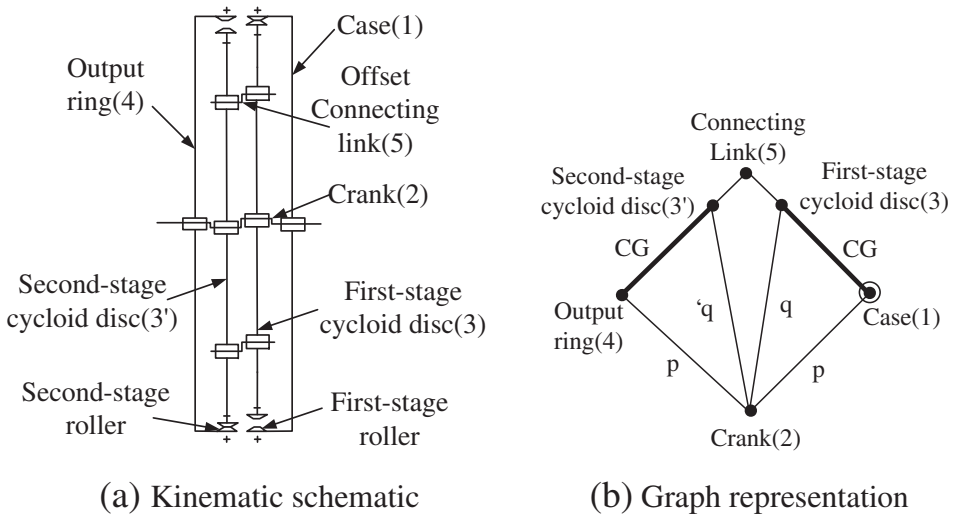

Fig. 5. Another different two-stage cycloidal drive.

It can be seen that the speed reduction ratio m can be maximized if the difference in teeth number between the first-stage and second-stage cycloidal discs is one and the teeth numbers of cycloidal discs maximize. Further, if $z_3 = z_3'$, which implies that the first-stage cycloidal train unit and the second-stage cycloidal train unit are identical, the output ring becomes stationary as the case (link 1).

3. Profile generation and modification

3.1. Profile generation

The generation of the cycloidal gear profile has been studied by many researchers [1–6]. In this Section, the coordinate systems and formula will be established in order for profile modification use in the later Section. As shown in Fig. 6, coordinate systems S_f (x_f–O_f–y_f), S_1 (x_1–O_1–y_1), and S_2 (x_2–O_2–y_2) respectively represents the coordinate system fixed on the frame, circular roller, and cycloidal disc. In the figure, θ_1 is the rotation angle of S_1 with respect to S_f, θ_2 is the rotation angle of S_2 with respect to S_f, a is the eccentricity (distance O_1O_f), r_p is the roller position (distance from roller center to O_1), r_{rp} is the radius of the roller, P is the contact point between roller surface and cycloidal disc, and α is the parameter of the contact point P on the roller. Also note that since the roller is meshing with the cycloidal disc, the relation $\theta_2 = z_p\theta_1/z_c$ holds for θ_1 and θ_2, where z_c and z_p are respectively the

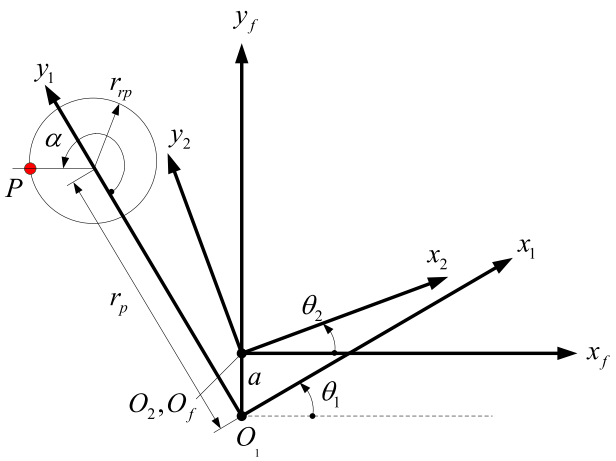

Fig. 6. Coordinate systems for profile generation.

number of teeth of cycloidal disc and number of rollers. Using the theory of gearing, the profile equation of the cycloidal disc can be obtained via the coordinate transformation and the equation of meshing:

$$\mathbf{r}_2(\alpha,\theta_1)=\mathbf{M}_{21}(\theta_1)\mathbf{r}_1(\alpha) \tag{4}$$

$$f(\alpha,\theta_1)=\left(\frac{\partial \mathbf{r}_2(\alpha,\theta_1)}{\partial\alpha}\times\mathbf{k}\right)\cdot\frac{\partial \mathbf{r}_2(\alpha,\theta_1)}{\partial\theta_1}=0 \tag{5}$$

where $\mathbf{r}_1=[r_{rp}\sin\alpha,\ r_p-r_p\cos\alpha,\ 0,\ 1]^T$ is the coordinate of P in S_1, $\mathbf{M}_{21}$ is the transformation matrix transforming system S_1 to system S_2, $\mathbf{r}_2$ is the coordinate of P in S_2 and $\mathbf{k}=[0,\ 0,\ 1]^T$ is the unit vector of z-axis. After substituting $\mathbf{r}_1$ into the above equations and solving the equation of meshing, one can obtain:

$$\mathbf{M}_{21}(\theta_1)=\mathbf{M}_{2f}\mathbf{M}_{f1}=\begin{bmatrix}\cos(\theta_1-\theta_2) & -\sin(\theta_1-\theta_2) & 0 & -a\sin\theta_2\\ \sin(\theta_1-\theta_2) & \cos(\theta_1-\theta_2) & 0 & -a\cos\theta_2\\ 0 & 0 & 1 & 0\\ 0 & 0 & 0 & 1\end{bmatrix} \tag{6}$$

$$\mathbf{r}_2(\alpha,\theta_1)=\mathbf{M}_{21}(\theta_1)\mathbf{r}_1(\alpha)=\begin{bmatrix}-r_p\sin\left(\left(1-\frac{z_p}{z_c}\right)\theta_1\right)-r_{rp}\sin\left(\alpha+\left(1-\frac{z_p}{z_c}\right)\theta_1\right)-a\sin\frac{z_p\theta_1}{z_c}\\ r_p\cos\left(\left(1-\frac{z_p}{z_c}\right)\theta_1\right)+r_{rp}\cos\left(\alpha+\left(1-\frac{z_p}{z_c}\right)\theta_1\right)-a\cos\frac{z_p\theta_1}{z_c}\\ 0\\ 1\end{bmatrix} \tag{7}$$

$$\alpha=\tan^{-1}\frac{-az_p\sin\theta_1}{r_p\left(z_c-z_p\right)+az_p\cos\theta_1}. \tag{8}$$

Once the design parameters r_p, r_{rp}, z_p, z_c, and a are given, Eqs. (7) and (8) can be used to generate cycloidal profiles.

3.2. Profile modification

Due to errors of assembly and manufacture, it is necessary to modify the cycloidal gear profile to compensate for those errors. Similar to involute gears, the modification of cycloidal gear profile may take account of crowning of gears in the longitudinal and profile directions. However, the thickness of the cycloidal disc is usually small compared to other dimensions in the disc and thus errors due to non-parallel shaft angle can be negligible. Therefore, only the modification of the profile will be considered. Because eccentricity a is small and its error can be incorporated into r_p and r_{rp}, parameters that may influence the profile are then the roller radius r_p and roller position r_{rp}. Sensinger [9] qualitatively showed that the topographic profile modified by roller position is different from that by roller radius. Therefore, to see how the modifications in fact affect the accuracy of the gear drive, in this work the profile modification will be investigated quantitatively by individual conditions as well as the compound condition.

Case a. Modification by roller radius r_{rp}
In this type of modification, the result can be obtained by adding a small quantity of Δr_{rp} to r_{rp} in the profile Eq. (7). Thus, a positive value of Δr_{rp} $(+\Delta r_{rp})$ will generate a profile with smaller tooth thickness than that of the nominal profile, resulting in clearance between the roller surface and cycloidal tooth surface. On the other hand, a negative value of Δr_{rp} $(-\Delta r_{rp})$ will generate a profile with a larger tooth thickness and yield interference between rollers and cycloidal disc.
Case b. Modification by roller position r_p
In this type of modification, the result can be obtained by adding a small quantity of Δr_p to r_p in the profile Eq. (7). In contrast to Case (a), $+\Delta r_p$ will generate a larger profile while $-\Delta r_p$ will generate a smaller profile.
Case c. Compound modifications by r_{rp} and r_p
In this type of modification, small values of roller radius, Δr_{rp}, and roller position, Δr_p, will both be added to Eq. (7). Since modification by $-\Delta r_{rp}$ and $+\Delta r_p$ will obtain an even larger profile and yield interference while modification by $+\Delta r_{rp}$ and $-\Delta r_p$ will obtain an even smaller profile and yield excessive clearance, these compound modifications are not practical in application. Thus, only modifications by $(+\Delta r_{rp},+\Delta r_p)$ and $(-\Delta r_{rp},-\Delta r_p)$ will be investigated in the later Section.

3.3. Flank topographic differences of the tooth profile

The flank topographic differences of the modified profile when compared with those of the theoretical profile can be obtained along the normals of sampled grid points. Referring to Fig. 7, steps for such derivation can be summarized as follows [25]:

Step 1 Positions $\mathbf{R}_{gT}^{(i,j)}$ and normals $\mathbf{n}_{gT}^{(i,j)}$ of the grid points on the theoretical tooth surface are obtained from the derived mathematical model of tooth surface, the given cycloidal gear parameters and the defined plane grids (i, j).
Step 2 Determine the positions of grid points on the modified tooth surface, $\mathbf{R}_{gA}^{(i,j)}$.

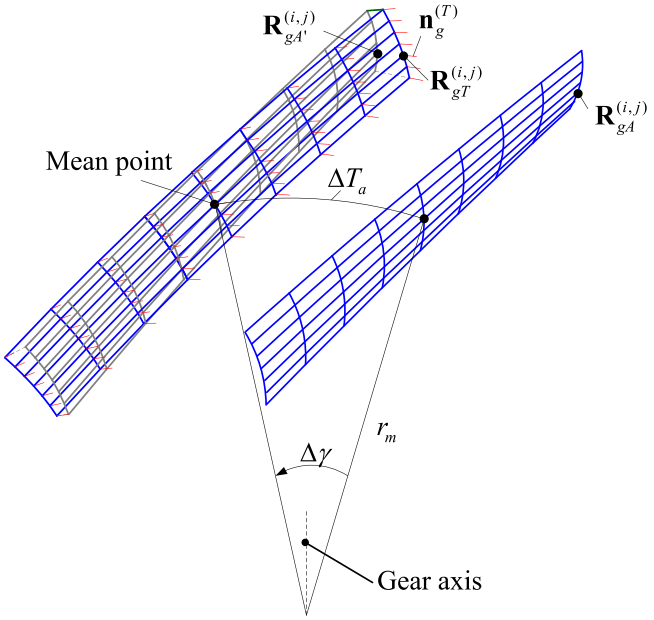

Fig. 7. Tooth thickness difference.

Step 3 Omit the backlash by rotating surface $\mathbf{R}_{gA}{}^{(i,j)}$ into $\mathbf{R}_{gA'}^{(i,j)}$ until its mean point coincides with that of the theoretical surface.
Step 4 Determine the normal deviations of the surface points between the actual and theoretical as follows:

$$e_n^{(i,j)} = \left(\mathbf{R}_{gA'}^{(i,j)} - \mathbf{R}_{gT}^{(i,j)}\right) \cdot \mathbf{n}_{gT}^{(i,j)}. \tag{9a}$$

Step 5 Determine the tooth thickness difference

$$\Delta T_a = r_m \Delta\gamma \tag{9b}$$

where r_m is the mean radius of gear, and $\Delta\gamma$ is the deviation of thickness angle.

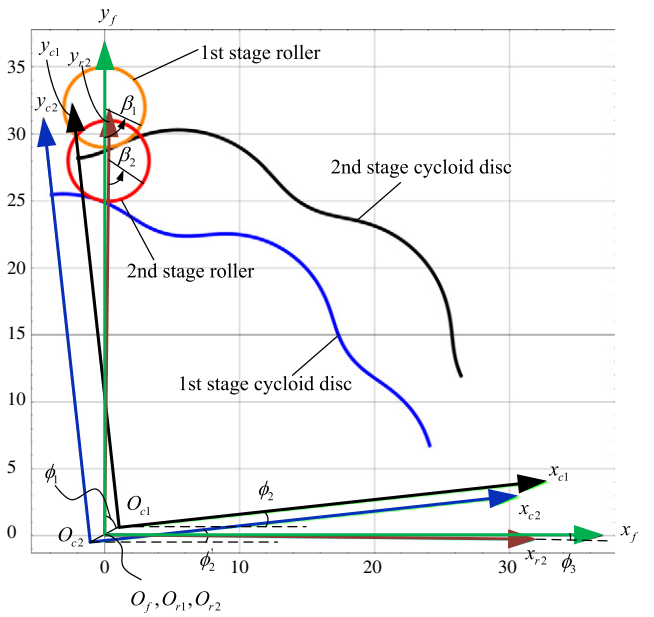

Fig. 8. Coordinate systems for TCA.

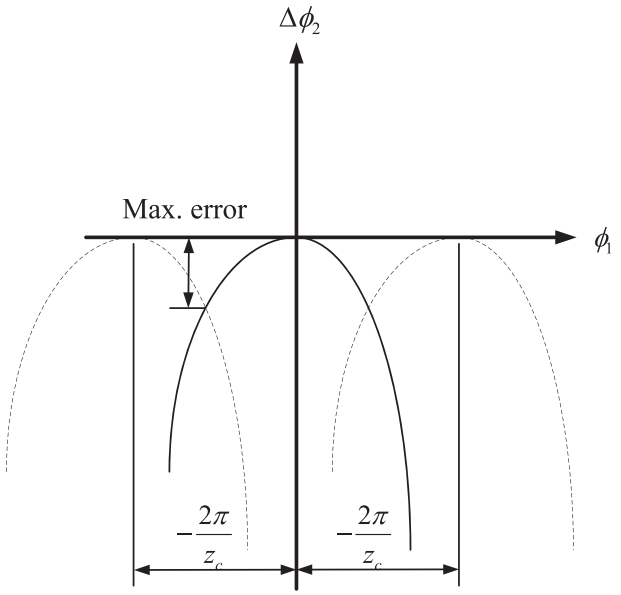

Fig. 9. Kinematic error.

3.4. Tooth contact analysis

The tooth contact analysis (TCA) can provide information about the surface contact condition at every instant and simulate the transmission errors caused by profile modification [18]. Before proceeding TCA, coordinate systems for assembly must be defined. As shown in Fig. 8, coordinate systems S_{c1} and S_{r1} are respectively the coordinate system attached to the 1st-stage cycloidal disc and its mating roller; coordinate systems S_{c2} and S_{r2} are respectively the coordinate system attached to the 2nd-stage cycloidal disc and its mating roller; and S_f is the fixed frame for assembly. Note that S_{r1} coincides with S_f. In addition, ϕ_1 is the crank input;

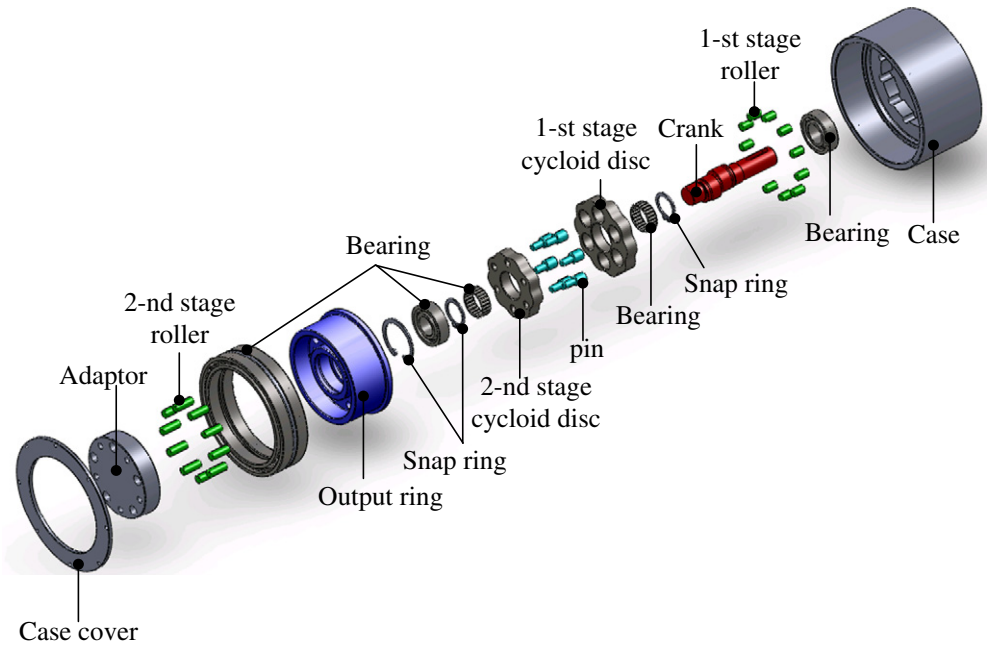

Fig. 10. Exploded View of the mechanism.

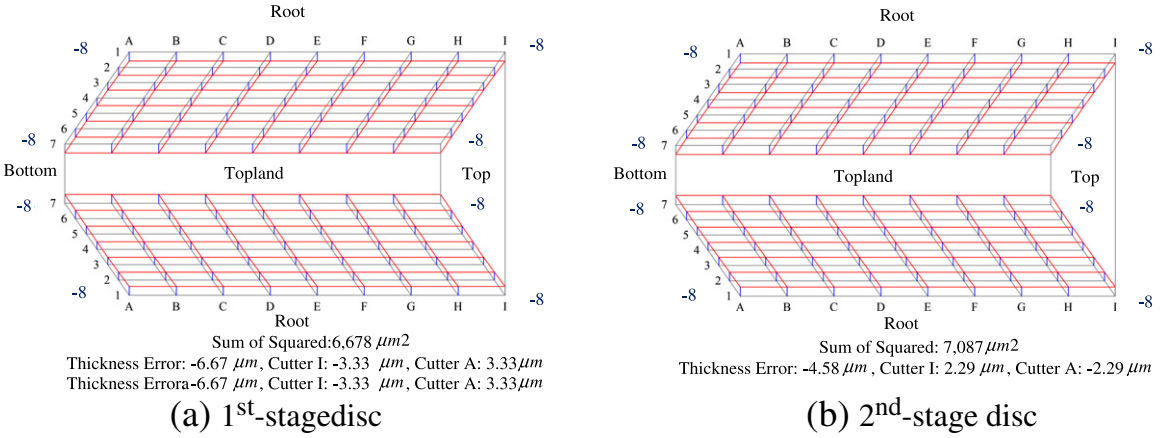

Fig. 11. Flank topographic difference of the profile.

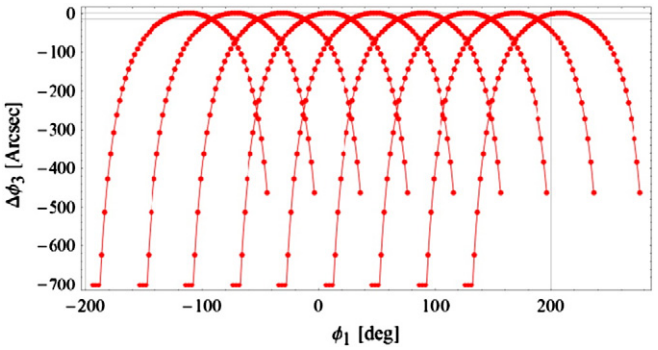

Fig. 12. Kinematic error, max. = 16.14 arcsec.

ϕ_2 and ϕ_2' are respectively the angle for the 1st-stage and 2nd-stage discs; and ϕ_3 is the angle of output link. In this work, the coordinates will be expressed with respect to the frame while performing TCA. Therefore, the following transformation matrices can be established:

$$\mathbf{M}_{fc1} = \begin{bmatrix} \cos\phi_2 & -\sin\phi_2 & 0 & \text{asin}\phi_1 \\ \sin\phi_2 & \cos\phi_2 & 0 & \text{acos}\phi_1 \\ 0 & 0 & 1 & 0 \\ 0 & 0 & 0 & 1 \end{bmatrix} \tag{10}$$

$$\mathbf{M}_{fc2} = \begin{bmatrix} \cos\phi_2' & -\sin\phi_2' & 0 & \text{asin}(\phi_1+\pi) \\ \sin\phi_2' & \cos\phi_2' & 0 & \text{acos}(\phi_1+\pi) \\ 0 & 0 & 1 & 0 \\ 0 & 0 & 0 & 1 \end{bmatrix} \tag{11}$$

$$\mathbf{M}_{fr2} = \begin{bmatrix} \cos\phi_3 & \sin\phi_3 & 0 & 0 \\ -\sin\phi_3 & \cos\phi_3 & 0 & 0 \\ 0 & 0 & 1 & 0 \\ 0 & 0 & 0 & 1 \end{bmatrix}. \tag{12}$$

Table 1
Maximum kinematic errors due to roller radius modifications.

Modification (mm)	$\Delta r_{rp} = 0.008$	$\Delta r_{rp} = 0.01$	$\Delta r_{rp} = 0.012$	$\Delta r_{rp} = 0.015$	$\Delta r_{rp} = 0.018$
Max. error (arcsec)					
Left flank	16.14	19.97	23.6	29.54	35.87
Right flank	15.59	19.55	23.42	29.29	35.27

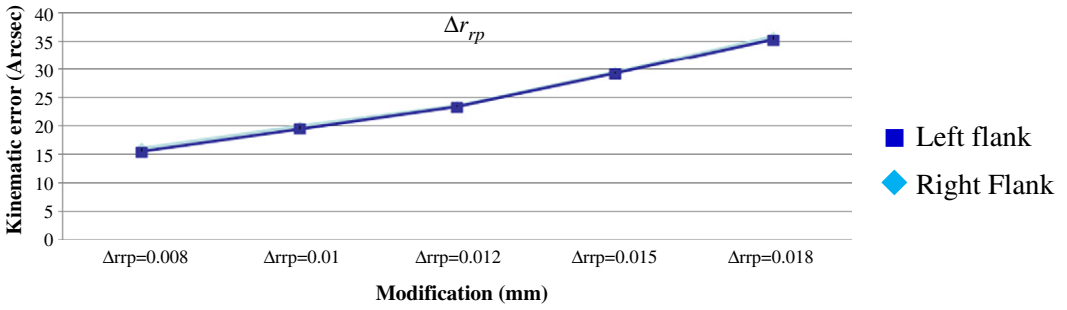

Fig. 13. Error trend due to roller radius modifications.

Rewrite the profile Eq. (7) for the 1st-stage cycloidal disc with modification as

$$\mathbf{r}_{c1}(\alpha_1,\theta_1) = \begin{bmatrix} -\left(r_{p1}+\Delta r_p\right)\sin\left(\left(1-\frac{z_{p1}}{z_{c1}}\right)\theta_1\right)-\left(r_{rp}+\Delta r_{rp}\right)\sin\left(\alpha_1+\left(1-\frac{z_{p1}}{z_{c1}}\right)\theta_1\right)-a\sin\frac{z_{p1}\theta_1}{z_{c1}} \\ \left(r_{p1}+\Delta r_p\right)\cos\left(\left(1-\frac{z_{p1}}{z_{c1}}\right)\theta_1\right)+\left(r_{rp}+\Delta r_{rp}\right)\cos\left(\alpha_1+\left(1-\frac{z_{p1}}{z_{c1}}\right)\theta_1\right)-a\cos\frac{z_{p1}\theta_1}{z_{c1}} \\ 0 \\ 1 \end{bmatrix} \tag{13}$$

in which $\alpha_1 = \tan^{-1}\left(\frac{-a\,z_{p1}\sin\theta_1}{\left(r_{p1}+\Delta r_p\right)\left(z_{c1}-z_{p1}\right)+a\,z_{p1}\cos\theta_1}\right)$. The position of contact point on the roller of the 1st-stage cycloidal drive is $\mathbf{r}_{r1} = [r_{rp}\sin\beta_1,\ r_p - r_{rp}\cos\beta_1,\ 0,\ 1]^T$. Similarly, the profile equation for the 2nd-stage cycloidal equation with modification can be rewritten as

$$\mathbf{r}_{c2}(\alpha_2,\theta_2) = \begin{bmatrix} -\left(r_{p2}+\Delta r_p\right)\sin\left(\left(1-\frac{z_{p2}}{z_{c2}}\right)\theta_2\right)-\left(r_{rp}+\Delta r_{rp}\right)\sin\left(\alpha_2+\left(1-\frac{z_{p2}}{z_{c2}}\right)\theta_2\right)-a\sin\frac{z_{p2}\theta_2}{z_{c2}} \\ \left(r_{p2}+\Delta r_p\right)\cos\left(\left(1-\frac{z_{p2}}{z_{c2}}\right)\theta_2\right)+\left(r_{rp}+\Delta r_{rp}\right)\cos\left(\alpha_2+\left(1-\frac{z_{p2}}{z_{c2}}\right)\theta_2\right)-a\cos\frac{z_{p2}\theta_2}{z_{c2}} \\ 0 \\ 1 \end{bmatrix} \tag{14}$$

in which $\alpha_2 = \tan^{-1}\left(\frac{-a\,z_{p2}\sin\theta_2}{\left(r_{p2}+\Delta r_p\right)\left(z_{c2}-z_{p2}\right)+a\,z_{p2}\cos\theta_2}\right)$. The position of contact point on the roller of the 2nd-stage cycloidal drive is $\mathbf{r}_{r2} = [r_{rp}\sin\beta_2,\ r_p - r_{rp}\cos\beta_2,\ 0,\ 1]^T$. Meanwhile, the contact normals of the cycloidal disc, $\mathbf{n}_{c1}$, and roller, $\mathbf{n}_{r1}$, for the 1st-stage cycloidal unit can be derived by

$$\mathbf{n}_{c1}(\alpha_1,\theta_1) = \frac{\frac{\partial \mathbf{r}_{c1}(\alpha_1,\theta_1)}{\partial\alpha_1}\times\mathbf{k}}{\left|\frac{\partial \mathbf{r}_{c1}(\alpha_1,\theta_1)}{\partial\alpha_1}\times\mathbf{k}\right|} \quad \text{and} \quad \mathbf{n}_{r1} = \frac{\frac{\partial \mathbf{r}_{r1}}{\partial\beta_1}\times\mathbf{k}}{\left|\frac{\partial \mathbf{r}_{r1}}{\partial\beta_1}\times\mathbf{k}\right|}. \tag{15}$$

Table 2
Maximum kinematic errors due to roller position modifications.

Modification (mm)	$\Delta r_{p1,2} = -0.016$	$\Delta r_{p1,2} = -0.0205$	$\Delta r_{p1,2} = -0.025$	$\Delta r_{p1,2} = -0.032$	$\Delta r_{p1,2} = -0.039$
Max. error (arcsec)					
Left flank	34.22	43.49	52.95	67.44	83.71
Right flank	33.02	41.8	51.71	67	80.37

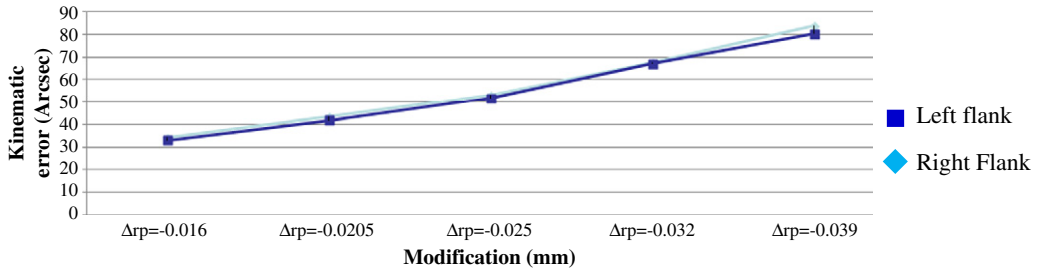

Fig. 14. Error trend due to roller position modifications.

Similarly, the contact normals of the cycloidal disc, $\mathbf{n}_{c2}$, and roller, $\mathbf{n}_{r2}$, for the 2nd-stage cycloidal unit can be derived as

$$\mathbf{n}_{c2}(\alpha_2,\theta_2)=\frac{\dfrac{\partial \mathbf{r}_{c2}(\alpha_2,\theta_2)}{\partial\alpha_2}\times\mathbf{k}}{\left|\dfrac{\partial \mathbf{r}_{c2}(\alpha_2,\theta_2)}{\partial\alpha_2}\times\mathbf{k}\right|}\quad\text{and}\quad\mathbf{n}_{r2}=\frac{\dfrac{\partial \mathbf{r}_{r2}}{\partial\beta_2}\times\mathbf{k}}{\left|\dfrac{\partial \mathbf{r}_{r2}}{\partial\beta_2}\times\mathbf{k}\right|}. \tag{16}$$

Thus, a family of cycloidal tooth and roller surfaces can be generated in the fixed coordinate system S_f by the matrix transformation

$$^{f}\mathrm{r}(\alpha_1,\theta_1,\phi_1,\phi_2)=\mathrm{M}_{fc1}(\phi_1,\phi_2)\mathrm{r}_{c1}(\alpha_1,\theta_1) \tag{17}$$

$$^{f}\mathbf{r}(\alpha_2,\theta_2,\phi_1,\phi_2)=\mathbf{M}_{fc2}(\phi_1,\phi_2')\mathbf{r}_{c2}(\alpha_2,\theta_2) \tag{18}$$

$$^{f}\mathbf{r}(\beta_1)=\mathbf{r}_{r1}(\beta_1) \tag{19}$$

$$^{f}\mathbf{r}(\phi_3,\beta_2)=\mathbf{M}_{fr2}(\phi_3)\mathbf{r}_{r2}(\beta_2). \tag{20}$$

Likewise, the unit normals to contact surfaces can be represented in S_f by the matrix equations

$$^{f}\mathbf{n}(\alpha_1,\theta_1,\phi_1,\phi_2)=\mathbf{L}_{fc1}(\phi_1,\phi_2)\mathbf{n}_{c1}(\alpha_1,\theta_1) \tag{21}$$

$$^{f}\mathbf{n}(\alpha_2,\theta_2,\phi_1,\phi_2)=\mathbf{L}_{fc2}\left(\phi_1,\phi_2'\right)\mathbf{n}_{c2}(\alpha_2,\theta_2) \tag{22}$$

$$^{f}\mathbf{n}(\beta_1)=\mathbf{n}_{r1}(\beta_1) \tag{23}$$

$$^{f}\mathbf{n}(\phi_3,\beta_2)=\mathbf{L}_{fr2}(\phi_3)\mathbf{n}_{r2}(\beta_2) \tag{24}$$

where $\mathbf{L}$ is a 3×3 matrix which is the upper left 3×3 submatrix of matrix $\mathbf{M}$. The condition for the continuous contact of the surfaces requires contact surfaces be in continuous tangency, i.e., their contact position vectors and normals coincide at any instant. And parameters (α_1,θ_1) and (α_2,θ_2) satisfy the equation of meshing. Thus,for the first-stage:

$$^{f}\mathbf{r}(\beta_1)=^{f}\mathbf{r}(\phi_1,\phi_2,\theta_1) \tag{25}$$

$$^{f}\mathbf{n}(\beta_1)=^{f}\mathbf{n}(\phi_1,\phi_2,\theta_1) \tag{26}$$

Table 3
Maximum kinematic errors due to positive roller radius and positive roller position modifications.

Modification (mm)	$\Delta r_{rp}=0.018$ $\Delta r_{p1,2}=0.016$	$\Delta r_{rp}=0.024$ $\Delta r_{p1,2}=0.0205$	$\Delta r_{rp}=0.03$ $\Delta r_{p1,2}=0.025$	$\Delta r_{rp}=0.039$ $\Delta r_{p1,2}=0.032$	$\Delta r_{rp}=0.048$ $\Delta r_{p1,2}=0.039$
Max. error (arcsec)					
Left flank	2.33	4.85	7.18	10.45	13.73
Right flank	2.11	4.46	6.92	10.07	13.03

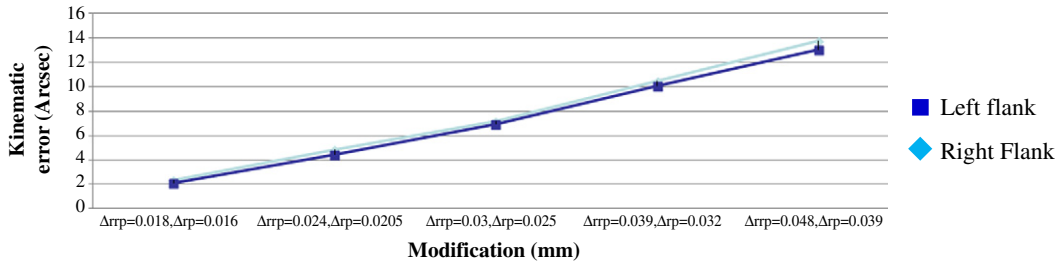

Fig. 15. Error trend of Table 3.

and for the second-stage:

$$^{f}\mathbf{r}(\phi_3,\beta_2) = {}^{f}\mathbf{r}\left(\phi_1,\phi_2^{'},\theta_2\right) \tag{27}$$

$$^{f}\mathbf{n}(\phi_3,\beta_2) = {}^{f}\mathbf{n}\left(\phi_1,\phi_2^{'},\theta_2\right). \tag{28}$$

It can be seen that Eqs. (25) and (26) provide three independent equations in three unknowns, ϕ_2, θ_1, and β_1, and one known crank input ϕ_1. Thus, tooth contact for the 1st-stage cycloidal disc can be solved. Then, Eqs. (27) and (28) also provide three independent equations in four unknowns, ϕ_2', θ_2, ϕ_3 and β_2. Note that ϕ_2' is identical with ϕ_2. Therefore, tooth contact for the 2nd-stage cycloidal disc can also be solved. Detailed expressions for Eqs. (25)–(28) can be referred to [23]. Once the output angle ϕ_3 is obtained, the transmission error $\Delta\phi_3$ can be written as the difference between the simulated, ϕ_3, and theoretical output, ϕ_3, namely,

$$\Delta\phi_3 = \phi_3 - m\phi_1. \tag{29}$$

Since the error in the circular pitch of the cycloidal tooth is not considered, the transmission error for adjacent teeth can be obtained by shifting the curve of Eq. (29) a period of $2\pi/z_c$, yielding a periodic curve as shown in Fig. 9. The maximum transmission error occurs at the position where two periodic curves intersect.

4. Mock-up design and TCA simulation

4.1. Design goal

A mock-up is designed to validate the feasibility of the new mechanism according to the above design procedure. The major design parameters are listed as below and will be used for TCA.

(a) Speed reduction ratio $m = 100$.
(b) First stage cycloidal train unit: number of rollers $z_{p1} = 11$, number of teeth of cycloidal disc $z_{c1} = 10$, roller position $r_{p1} = 32$ mm, roller radius $r_{rp} = 3$ mm, eccentricity $a = 1.2$ mm.
(c) Second stage cycloidal train unit: number of rollers $z_{p2} = 10$, number of teeth of cycloidal disc $z_{c2} = 9$, roller position $r_{p2} = 28$ mm, roller radius $r_{rp} = 3$ mm, eccentricity $a = 1.2$ mm.

The exploded view of the mechanism is shown in Fig. 10.

4.2. Simulation results of TCA

Using Eqs. (25)–(28), the simulation of TCA is performed. The quantity of modification is determined based on the ISO tolerance system [24]. Thus, the results of modifications can be compared on a reference when different design parameters are employed. As an example, Fig. 11 shows the results of the flank topographic surface difference and Fig. 12 is the kinematic error of

Table 4
Maximum kinematic errors due to negative roller radius and negative roller position.

Modification (mm)	$\Delta r_{rp} = -0.008$ $\Delta r_{p1,2} = -0.016$	$\Delta r_{rp} = -0.01$ $\Delta r_{p1,2} = -0.0205$	$\Delta r_{rp} = -0.012$ $\Delta r_{p1,2} = -0.025$	$\Delta r_{rp} = -0.015$ $\Delta r_{p1,2} = -0.032$	$\Delta r_{rp} = -0.018$ $\Delta r_{p1,2} = -0.039$
Max. error (arcsec)					
Left flank	17.58	23.19	28.59	37.14	46.09
Right flank	17.46	23.11	27.97	37.03	44.91

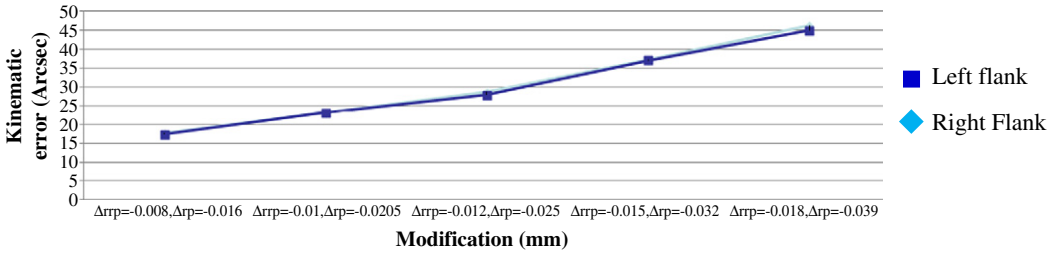

Fig. 16. Error trend of Table 4.

the output of which the maximum error is 16.14 arcsec, if the quantity of modification $\Delta r_{rp} = +0.008$ mm and $\Delta r_p = 0$ is employed. In what follows, the results of TCA for various types of modifications will be illustrated.

(a) Positive roller radius modification, $r_{rp} = 3$ mm. Five values of Δr_{rp} extracted from IT6 (International Tolerance Grade 6), IT7, IT8 and their interpolations of r_{rp} are employed. Table 1 lists the maximum kinematic errors that the cycloidal drive can generate. Fig. 13 shows the trend of curves of the errors.

(b) Negative roller position modification, $r_{p1} = 32$ mm. Similarly, five values are employed for simulation, which are from max values of IT6, IT7, IT8, and their interpolations. Table 2 lists the maximum errors and Fig. 14 shows the trend of curves under such modification. It can be seen that a smaller quantity of modification may yield smaller kinematic errors in a single type of modification.

(c) Positive roller radius plus positive roller position. In this category, Δr_p chosen from IT6, IT7 and IT8 are combined with Δr_{rp} chosen from IT8, IT9 and IT10. Table 3 lists the results of maximum kinematic errors from compound modification and Fig. 15 shows the trend of error curves vs. modification values. Compared to type (a) modification, compound modification may yield smaller kinematic errors than single variable modification.

(d) Negative roller radius plus negative roller position. In this category, Δr_{p} chosen from IT6, IT7, and IT8 are combined with Δr_{rp} chosen from IT6, IT7, and IT8. Results of kinematic errors are listed in Table 4. Also, trend of error curves is shown in Fig. 16.

As seen from cases (c) and (d), if modification variables are appropriately selected a larger value of modification can still produce smaller kinematic errors.

Figs. 17–19 shows some pictures of the major parts manufactured. The reduction ratio is also validated via manual operation of the drive and the operation video can be seen on the website: http://www.youtube.com/watch?v=qZbO5kVdvtU.

5. Conclusion

This paper presents the new design of a two-stage cycloidal speed reducer. The topological analysis provides the designer more realization of the characteristics of the cycloidal speed reducers. Two new structures of two-stage cycloidal speed reducers are then enumerated after topological analysis. A new configuration with the least number of links and joints is chosen to establish the design procedure and a mock-up is fabricated to validate the feasibility of this type of two-stage cycloidal drive. The angular velocity analysis of the gear drive is straightforwardly obtained through the help of graph representation. Modifications of

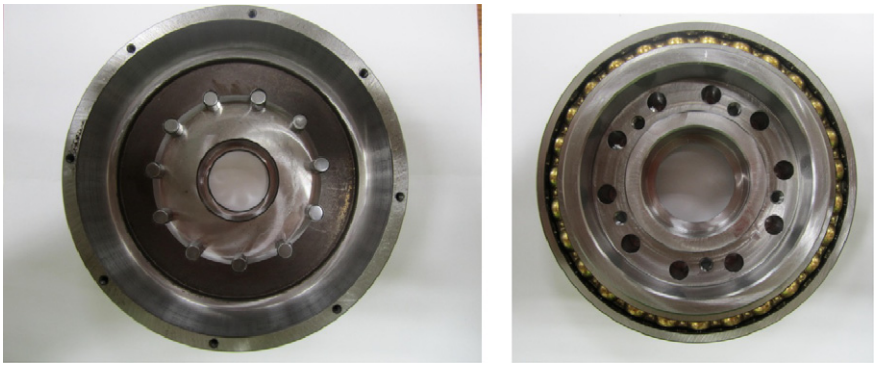

Fig. 17. Case and output ring.

(a) 1st-stage cycloidal disc (b) 2nd-stage cycloidal

Fig. 18. 1st-stage and 2nd-stage cycloidal discs.

(a) Crank (b) Roller

Fig. 19. Crank and roller.

the cycloidal gear profile and transmission errors are analyzed quantitatively rather than qualitatively. It is shown that a smaller quantity of modification in a single type of modification yields smaller kinematic errors. However, compound modifications may yield smaller kinematic errors than a single type of modification. Further, if variables for compound modification are appropriately selected, a larger value of modification can still acquire smaller kinematic errors. Based on the results obtained, this new cycloidal drive is realizable as a compact, high speed reduction ratio, and high accuracy speed reduction device.

Acknowledgment

The financial support of the National Science Council Taiwan (NSC 102-2221-E-002-048) is acknowledged.

References

[1] D.W. Botsiber, L. Kingston, Cycloid speed reducer, Mach. Des. (June) (1956) 65–69.
[2] E.P. Pollitt, Some applications of the cycloid in machine design, ASME J. Eng. Ind. (1960) 407–414.
[3] D.C.H. Yang, J.G. Blanche, Design and application guidelines for cycloid drives with machining tolerances, Mech. Mach. Theory 25 (5) (1990) 487–501.
[4] H.S. Yan, T.S. Lai, Geometry design of an elementary planetary gear train with cylindrical tooth-profiles, Mech. Mach. Theory 37 (2002) 757–767.
[5] T.S. Lai, Geometric design of roller drives with cylindrical meshing elements, Mech. Mach. Theory 40 (1) (2005) 55–57.
[6] C.F. Hsieh, Study on Geometry Design of Rotors Using Trochoidal Curve, (Ph.D. Dissertation) Department of Mechanical Engineering, National Chung Cheng University, Taiwan, 2006.
[7] Z.H. Fong, C.W. Tsay, Study on the undercutting of internal cycloidal gear with small tooth difference, J. CSME 21 (4) (2000) 359–367.
[8] C.F. Hsieh, Y.W. Hwang, Geometric design using hypotrochoid and nonundercutting conditions for an internal cycloidal gear, ASME J. Mech. Des. 129 (2007) 413–420.
[9] J.W. Sensinger, Unified approach to cycloid drive profile, stress, and efficiency optimization, ASME J. Mech. Des. 132 (2010) 024503-1~5.
[10] J.G. Blanche, D.C.H. Yang, Cycloid drives with machining tolerances, ASME J. Mech., Trans., and Auto. in Des. 111 (1989) 337–344.
[11] C.S. Huang, On the Surface Design, Tooth Contact Analysis, and Optimum Design of Cycloidal Drives with Modified Tooth Profiles, (M.S. Thesis) Department of Mechanical Engineering, National Cheng Kung University, Taiwan, 2006.
[12] S.K. Malhotra, M.A. Parameswaran, Analysis of a cycloid speed reducer, Mech. Mach. Theory 18 (6) (1983) 491–499.
[13] C. Gorla, P. Davoli, F. Rosa, C. Longoni, F. Chiozzi, A. Samarani, Theoretical and experimental analysis of a cycloidal speed reducer, ASME J. Mech. Des. 130 (2008) 112604-1~8.
[14] Janek, B. "Gear system," US Patent No. 5908372, Jun (1999).
[15] Nakamura, K. "Speed reduction device," US Patent No. 7811193B2, Oct (2010).
[16] X. Li, W. He, L. Li, L.C. Schmidt, A new cycloid drive with high-load capacity and high efficiency, ASME J. Mech. Des. 126 (4) (2004) 683–686.
[17] M. Blagojevic, N. Marjanovic, Z. Djordjevic, B. Stojanovic, A. Disic, A new design of a two-stage cycloidal speed reducer, ASME J. Mech. Des. 133 (2011) 085001-1~7.
[18] F.L. Litvin, A. Fuentes, Gear Geometry and Applied Theory, 2nd ed. Cambridge University Press, Cambridge, UK, 2004.
[19] L.W. Tsai, Mechanism Design — Enumeration of Kinematic Structures According to Function, CRC Press, 2001.
[20] H.S. Yan, Creative Design of Mechanical Devices, Springer-Verlag, Singapore, 1998.
[21] C.C. Chiu, Innovative Design and Analysis of Cycloidal Gear Reducers, (M.S. Thesis) Department of Mechanical Engineering, National Taiwan University, Taiwan, 2012.
[22] L.L.C. Onvio, Webpage, http://www.onviollc.com/objects/pdf/onvio_catalog_zero-backlash-speed-reducers.pdf.
[23] W.S. Lin, Kinematic Error Analysis and Design of a Two-Stage Cycloidal Drive, (M.S. Thesis) Dept. of Mech. Engr., National Taiwan University, Taiwan, 2013.
[24] F. Wang, Y. Yang, F. Chu, F. Kang, S. Jan, Engineering Graphics-CAD Communications, Chuan Hwa Science & Technology Book Co, Taiwan, 2007.
[25] Y.P. Shih, S.D. Chen, Free-form flank correction in helical gear grinding on a five-axis CNC gear profile grinding machine, ASME J. Manuf. Sci. E.-T. 134 (8) (2012) 041006-1–13.